Ocean Dynamics (2010) 60:171–180
DOI 10.1007/s10236-009-0257-7

A note on Stokes production of turbulence kinetic energy in the oceanic mixed layer: observations in the Baltic Sea

Lakshmi Kantha · Hans Ulrich Lass · Hartmut Prandke

Received: 24 July 2009 / Accepted: 2 December 2009 / Published online: 12 January 2010

Abstract Shear- and convection-driven turbulence coexists with wind-generated surface gravity waves in the upper ocean. The turbulent Reynolds stresses in the oceanic mixed layer can therefore interact with the shear of the wave-generated Stokes drift velocity to extract energy from the surface waves and inject it into turbulence, thus augmenting the mean shear-driven turbulence. Stokes production of turbulence kinetic energy (TKE) is difficult to measure in the field, since it requires simultaneous measurement of the turbulent stress and the Stokes drift profiles in the water column. However, it is readily inferred using second moment closure models of the oceanic mixed layer provided: (1) wave properties are available, along with the usual water mass properties, and radiative and air–sea fluxes needed to drive the mixed layer model and (2) the model skill can be assessed by comparing the model results against the observed dissipation rates of TKE. Comprehensive measurements made during the Reynolds 2002 campaign in the Baltic Sea have made the estimation of Stokes production possible, and in this paper, we report on the effort and the conclusions reached. Measurements of air–sea exchange parameters and water mass properties during the campaign allowed a mixed layer model to be run and the turbulent stress in the water column to be inferred. Simultaneous wave spectrum measurements enabled Stokes drift profile to be deduced and wave breaking to be included in the model run, and the Stokes production of TKE in the water column estimated. Direct measurements of the TKE dissipation rate from an upward traversing microstructure profiler were used to assure that the model could reproduce the turbulent dissipation rate in the water column. The model results indicate that the Stokes production of TKE in the mixed layer is of the same order of magnitude as the shear production and must therefore be included in mixed layer models.

Keywords Turbulence · Turbulent mixing · Stokes production · Wave turbulence interaction · Wind waves · Turbulence kinetic energy

Responsible Editor: Richard John Greatbatch

L. Kantha (✉)
Department of Aerospace Engineering Sciences,
University of Colorado,
Boulder, CO, USA
e-mail: kantha@colorado.edu

H. U. Lass
Baltic Sea Research Institute,
Warnemunde Rostock, Germany

H. Prandke
ISW Wassermesstechnik,
Petersdorf, Germany

1 Introduction

Conventional wisdom regards the momentum and buoyancy fluxes at the air–sea interface as being responsible for turbulence in the oceanic mixed layer. However, this ignores the fact that invariably, turbulence and wind-generated surface gravity waves co-exist in the upper ocean and therefore can and do interact with each other. The shear stresses in the oceanic mixed layer interact with the wave-generated Stokes drift to extract energy from surface waves and inject it into turbulence. This Stokes production of turbulence kinetic energy (TKE) enhances mixing (Kantha and Clayson 2004) in the oceanic mixed layer (OML), increases the entrainment at its bottom, and tends to make the profiles in the OML more uniform (Carniel et al. 2005). Stokes production is difficult to measure directly in the

field, since this requires simultaneous measurements of the turbulent shear stress and the Stokes drift profiles in the mixed layer. So are many quantities associated with turbulence except for the dissipation rates of TKE and temperature variance routinely measured by a microstructure profiler. While a shear probe can readily infer the dissipation rate of TKE, the measurement of quantities such as the shear stress and TKE budget requires turbulence sensors, not yet routinely deployed in the ocean. However, Stokes production is readily inferred using second moment closure models of turbulent mixing in the oceanic mixed layer incorporating Stokes production, provided: (1) wave properties needed to calculate the Stokes drift are available, along with the usual water mass properties and radiative and air–sea fluxes needed to drive the mixed layer model. Specifically, the wave spectrum needs to be measured in the vicinity so that the vertical profile of the Stokes drift can be deduced. (2) Microstructure profiler-measured TKE dissipation rates in the mixed layer are available from the air–sea interface to the OML bottom, to assure the model skill and thus provide confidence in the estimates. It is the goal of this paper to make use of a unique observational dataset from the Baltic Sea, and demonstrate that the Stokes production of TKE is of the same magnitude as the conventional shear production and hence quite important to OML dynamics. It is also important to the dissipation of wind-generated waves in the global ocean (Kantha 2006; Kantha et al. 2009).

In a typical field campaign, it is unlikely that mixed layer properties would be measured simultaneously with wave properties and turbulence in the mixed layer, as well as air–sea fluxes. A dedicated field campaign would be needed to gather the observational data necessary to infer Stokes production. The Reynolds 2001 and 2002 cruises in the Baltic Sea (Lass and Prandke 2003; Lass and Prandke, submitted for publication) were part of such a dedicated field campaign. The comprehensive measurements made during these cruises have enabled Stokes production of TKE to be inferred from a mixed layer model. The mixed layer model (Kantha and Clayson 2004) used is based on second moment closure of turbulence and includes turbulence produced by both wave breaking and Stokes production. In addition, during the campaign, a microstructure profiler was deployed from a research vessel anchored nearby and traversed up from below in order to measure the TKE dissipation rate in the water column close to the air–sea interface without any contamination. These measurements were used to assure model skill.

2 Observational dataset

Comprehensive measurements were made during three Reynolds cruises aboard the R/V *Prof. A. Penck* of the Baltic Research Institute of Germany. The first cruise (Reynolds 01) was from August 27, 2001 to September 8, 2001. The second cruise (Reynolds 02) took place between June 26, 2002 and July 8, 2002, while the third one (Reynolds 03) was from September 29, 2002 to October 11, 2002. Measurements were made at a location on the western slope of a shallow bank in the central Baltic Sea (Fig. 1), where the water column depth was about 50 m. This site was chosen since it made it possible to anchor the R/V and deploy the ascending dissipation profiler there in moderate wind speeds.

The principal suite of observations consisted of repeated measurements of the TKE dissipation rate using an ascending microstructure profiler (see Lass et al. 2003 for details of the microstructure profiler). The profiler was operated from the R/V via a controlled winch and a bottom-mounted idler pulley positioned approximately 100 m from the anchored ship (Fig. 2). A buoyancy body below the profiler pulled the cable out of the guide pulley and enabled the profiler to ascend freely from the bottom and measure the TKE dissipation rate all the way to the air–sea interface, without contamination from the wake of the anchored ship or the profiler itself (see Lass and Prandke 2003 for more details). Notice the slack between the freely ascending profiler and the buoyancy body. This slack is essential to isolate the profiler from the rest of the deployment mechanism. Just as in the case of a free falling profiler,

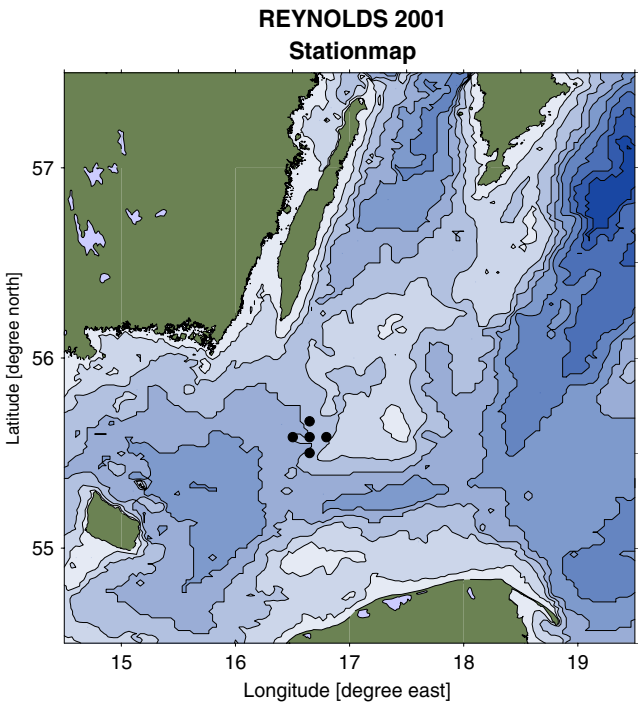

Fig. 1 Location map of the observational site in the Baltic Sea (figure taken from Lass and Prandke 2003). The *dots* indicate CTD stations. Microstructure measurements were made from R/V *Penck* anchored at the central station (see Fig. 2)

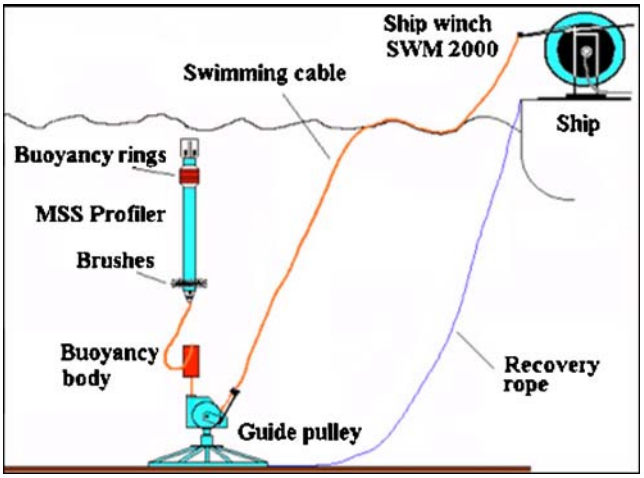

Fig. 2 Deployment of the raising microstructure profiler from R/V *Penck* anchored at the central station (figure taken from Lass and Prandke 2003)

the whole idea is to isolate the profiler from everything else so that it can ascend freely without any constraint from the buoyancy body, the cable or the winch.

The profiler had to be recovered and redeployed when substantial changes occurred in the wind direction. Wind speeds exceeding 12 m/s forced a halt in the dissipation measurements. Six profiles were taken every hour in a burst mode with a sampling time of approximately 5 min. The raw data were averaged over 0.25-m depth bins to yield hourly profiles of TKE dissipation rate in the water column.

Auxiliary measurements consisted of hourly time series of temperature, salinity, and fluorescence profiles taken with a CTD from the sea surface to close to the bottom. Hourly current profiles were measured with a bottom mounted 600 kHz RDI ADCP. The ADCP was configured to measure current vectors with 1-m vertical bin size by hourly bursts of 300 pings, which were vector averaged. Hourly surface wave spectra were calculated by means of pressure measurements recorded by a SBE 26 pressure sensor, moored about 5 m below the sea surface. Each pressure time series comprised 1,024 samples of 1-s averaged pressure measurements. Both the ADCP and the SBE26 were moored half a nautical mile from the ship. Lass and Prandke (2003) provide more details.

Momentum and buoyancy fluxes at the air-sea interface were calculated from the time series of meteorological parameters measured on board the R/V. The wind sensors were located on the mast 12 m above the sea surface; other sensors were at 9 m height. The meteorological measurements were adjusted to standard 10 m height assuming neutral stability and were averaged to hourly values. Incoming SW and LW radiative fluxes were also measured. The buoyancy flux at the air–sea interface was estimated from hourly mean values of the surface meteorological measurements of wind speed, air and water temperatures, humidity, pressure, sea surface temperature, and precipitation. More details on data collection and processing can be found in a paper being readied for publication (Lass and Prandke, submitted for publication). It describes observational results of the Reynolds campaign in some detail.

The wind forcing was characterized by calm phases punctuated by events of moderate strength during all three experiments. The buoyancy flux depicted a diurnal cycle with buoyancy gain during the day and a loss during the night. During Reynolds 01 and Reynolds 02 campaigns, the net buoyancy flux was directed into the sea, while there was a net loss of buoyancy during Reynolds 03. A strong thermocline existed at a depth of about 22 m. The mean currents were dominated by inertial oscillations and vertically propagating inertial waves. The vertical shear of the mean currents was maximum at the depth of the thermocline. For a more detailed description of the campaigns and the observational results, see Lass and Prandke, submitted for publication (see also Lass and Prandke 2003).

Collision with the R/V damaged the wave meter and the wave data are therefore unavailable for Reynolds 03. The wave spectra of Reynolds 01 were affected by pulse like motions from a surface float attached to the wave recorder at a depth of about 5 m. Therefore, only Reynolds 02 data are used in this study. The Stokes drift profile in each case was computed from the wave frequency spectrum using (Hasselmann 1970):

$$\vec{U}_S(z) = \int_0^\infty \frac{1}{g}(2\pi f)^3 E(f) \exp\left(-\frac{2}{g}(2\pi f)^2 z\right)\vec{k}\,df \qquad (1)$$

where f is the frequency in Hz, $E(f)$ is the measured power, g is the gravitational acceleration, $\vec{k}$ is the unit vector in the direction of wave propagation and z is the vertical coordinate positive upwards.

Stokes production of TKE is computed from:

$$P_{ST} = -\rho\overline{uw}\frac{\partial U_S}{\partial z} - \rho\overline{vw}\frac{\partial V_S}{\partial z} \qquad (2)$$

where $U_S(z)$ and $V_S(z)$ are the components of surface gravity wave field-induced Stokes drift velocity, $-\rho\overline{uw}$ and $-\rho\overline{vw}$ are components of the turbulent shear (Reynolds) stress; ρ is water density. Note that the expression for Stokes production is similar in form to that for the conventional shear production of TKE, except that the Stokes velocity shear replaces the mean shear.

3 Mixed layer model

The 1-D mixed layer model used in this study is that developed by Kantha and Clayson (2004). It is based on the

Mellor–Yamada type second moment closure of turbulence (Mellor and Yamada 1982, Galperin et al. 1988, Kantha and Clayson 1994). In this approach, the equations for second moment quantities of turbulence are reduced to a single differential equation for q^2 (twice the TKE) and algebraic relations for the second moments. In addition, since the minimum description of turbulence must consist of two quantities, its velocity scale (indicative of the energy contained in turbulent fluctuations) and its length scale (indicative of the scale of the energy containing eddies), the turbulence macroscale ℓ is derived through a conservation equation for $q^2\ell$. With the inclusion of the Stokes production terms, the q^2 equation is:

$$\frac{\partial}{\partial t}\left(q^2\right) - \frac{\partial}{\partial z}\left[q\ell S_q \frac{\partial}{\partial z}\left(q^2\right)\right] = -2\left(\overline{uw}\frac{\partial U}{\partial z} + \overline{vw}\frac{\partial V}{\partial z}\right) - 2\left(\overline{uw}\frac{\partial U_S}{\partial z} + \overline{vw}\frac{\partial V_S}{\partial z}\right) + 2\overline{wb} - 2\frac{q^3}{B_1\ell} \tag{3}$$

The equation for $q^2\ell$ is:

$$\frac{\partial}{\partial t}\left(q^2\ell\right) - \frac{\partial}{\partial z}\left[q\ell S_\ell \frac{\partial}{\partial z}\left(q^2\ell\right)\right] = E_1\ell\left(-\overline{uw}\frac{\partial U}{\partial z} - \overline{vw}\frac{\partial V}{\partial z}\right) + E_6\ell\left(-\overline{uw}\frac{\partial U_S}{\partial z} - \overline{vw}\frac{\partial V_S}{\partial z}\right) + E_3\overline{wb} - E_2\frac{q^3}{B_1}\left[1 + E_4\left(\frac{\ell}{\kappa\ell_w}\right)^2\right] \tag{4}$$

The first term on the right hand side of Eqs. 3 and 4 is the shear production, the second term is the Stokes production, and the third term is the buoyancy production/dissipation term. The last term is the dissipation term. E_1, E_2, E_3, E_4, and E_6 are closure constants, $\overline{wb}$ is the buoyancy flux. E_1=1.8, E_2=1, E_3=5, E_4=1.88, and E_6=7.2 (E_6 was mistakenly stated as 4.0 in Kantha and Clayson 2004). The model includes turbulence induced by breaking surface waves. For details on how wave breaking is modeled, see Kantha and Clayson (2004).

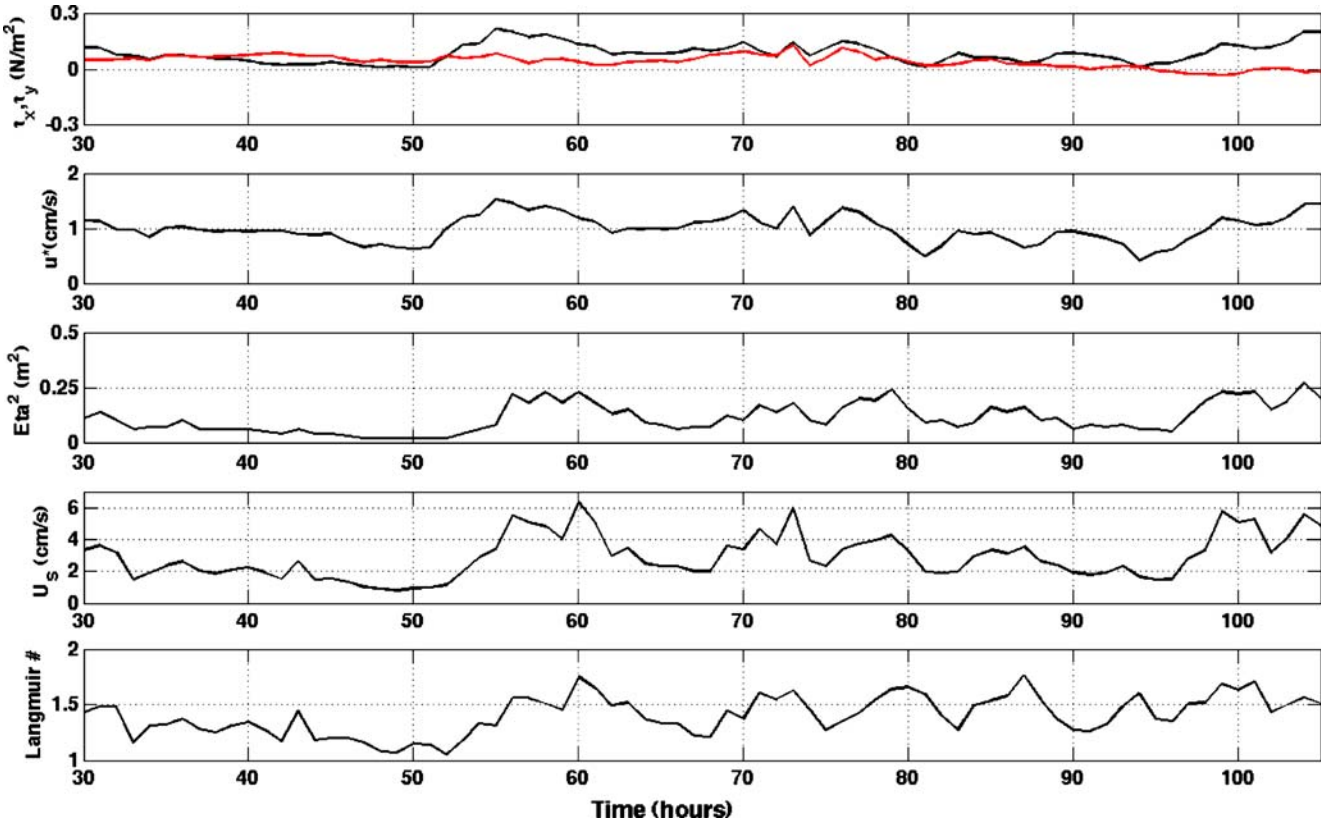

Fig. 3 The time series of the wind stress components τ_x, τ_y (*red*), friction velocity u^*, $\overline{\eta^2}$, the surface Stokes drift speed $\left|\vec{U}_S\right|$ and the Langmuir number *La*

An additional effect of the Stokes drift is the modification of the Coriolis terms in the momentum equations (McWilliams et al. 1997):

$$\frac{\partial U}{\partial t} - f(V + V_S) = -\frac{\partial}{\partial z}(\overline{uw})$$
$$\frac{\partial V}{\partial t} + f(U + U_S) = -\frac{\partial}{\partial z}(\overline{vw}) \quad (5)$$

These equations are solved along with equations for the mean temperature T and salinity S. More details can be found in Kantha and Clayson (1994, 2004).

The model was initialized using T & S data from CTD and velocities U and V from ADCP measurements at hour 29.5. The model was then driven by momentum and buoyancy fluxes derived from met data. The model time step was 15 min. Since the objective of the study is to

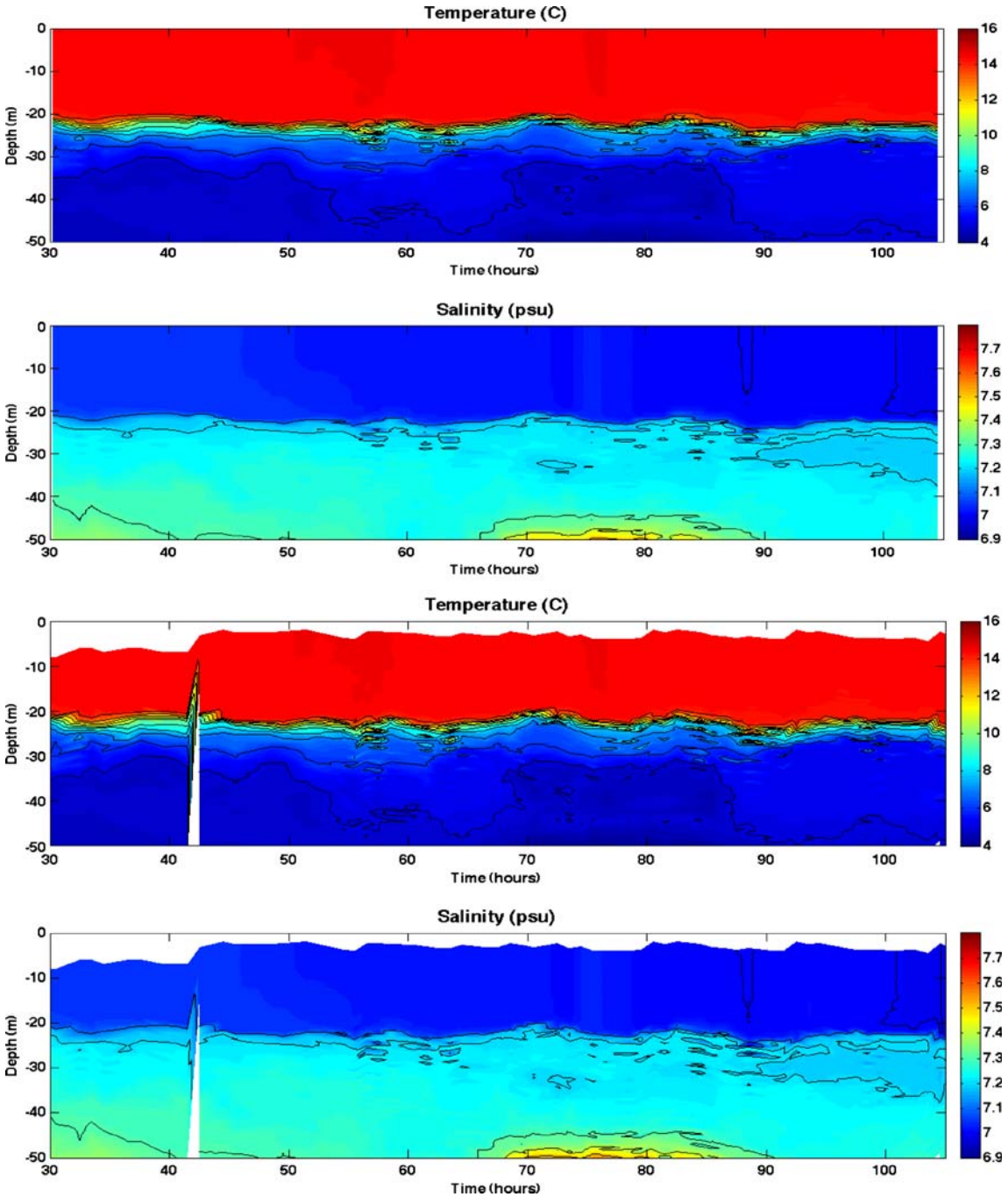

Fig. 4 Modeled temperature and salinity (*top two panels*) and observed temperature and salinity (*bottom two panels*) structure in the water column

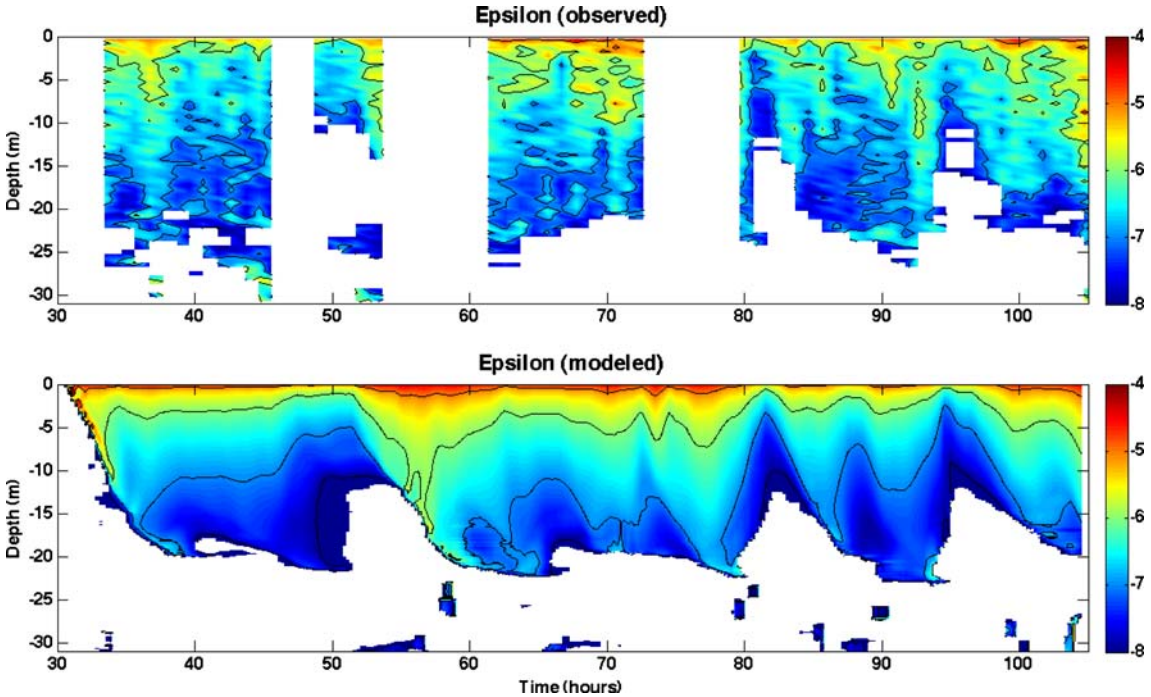

Fig. 5 Observed (*top*) and modeled (*bottom*) TKE dissipation rate (in W kg^{-1} or equivalently $m^2 s^{-3}$) in the water column, both shown on a logarithmic scale. The overall agreement is quite good. The model includes TKE injection by wave breaking at the surface and Stokes production of TKE (Case 4)

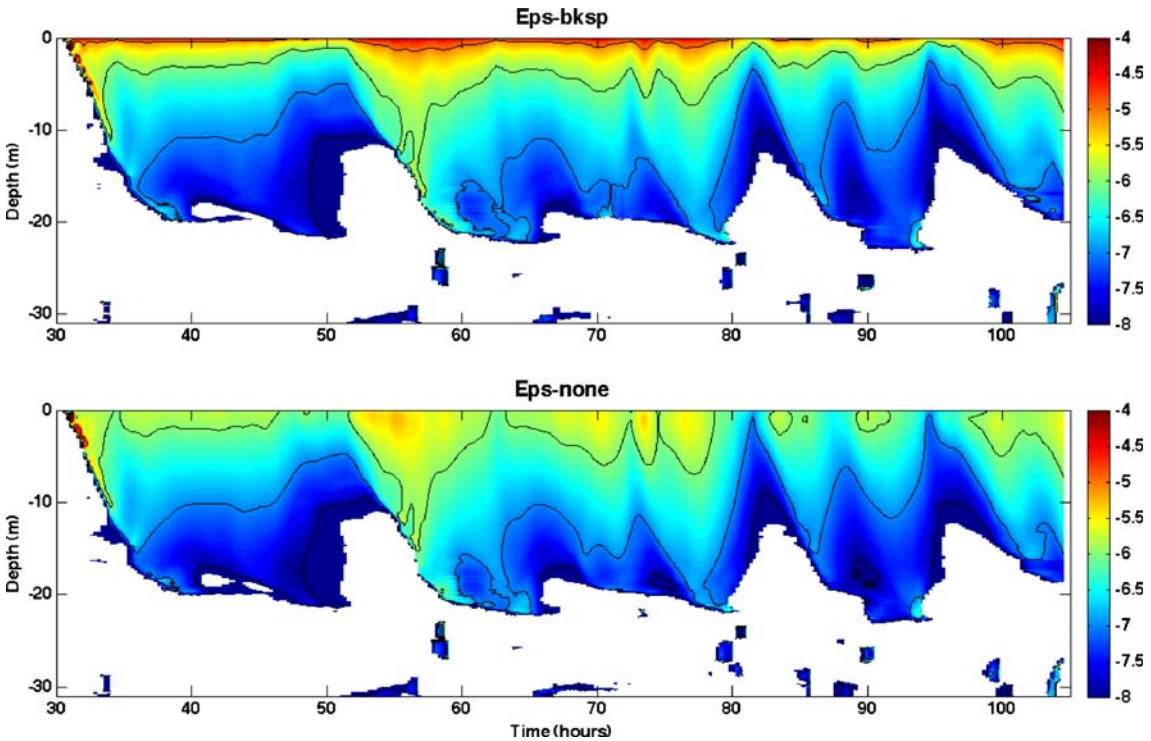

Fig. 6 Modeled TKE dissipation rate (in W kg^{-1}) (*top*) including TKE injection by wave breaking at the surface and Stokes production (Case 4) and (*bottom*) including neither (Case 1). Note the logarithmic scale. Note also that the latter does not agree as well with observed values (see Fig. 2)

simulate the turbulence in the water column as accurately as possible, it is necessary to reproduce the density structure of the water column as accurately as possible. To do this, *T* & *S* data from the CTD casts were assimilated into the model. The model was run continuously and through the gaps in microstructure observations. The shear stress was computed using

$$\overline{uw} = -K_M \frac{\partial U}{\partial z}; \overline{vw} = -K_M \frac{\partial V}{\partial z} \quad (6)$$

where K_M is the eddy viscosity, determined from the turbulence closure model (see Kantha and Clayson 1994, 2004 for details).

Four model runs were made: (1) without wave breaking or Stokes production, (2) with wave breaking only, (3) with Stokes production only, and (4) with both wave breaking and Stokes production effects included (the base case). These four runs are designed to elucidate the influence of wave breaking and shear production on turbulence, specifically the TKE dissipation rate. Wave breaking is included so as to simulate the OML as realistically as possible, even though it is the Stokes production that is the focus of this study.

4 The results

Figure 3 shows the time series of the wind stress components τ_x, τ_y, friction velocity u^*, the surface Stokes drift speed $|\vec{U}_S|$, $\overline{\eta^2}$, and the Langmuir number *La* defined as $La = \left(\frac{u_*^2|\vec{U}_s|}{u_*^3}\right)^{1/3} = \left(\frac{|\vec{U}_S|}{u_*}\right)^{1/3}$ since $\vec{\tau}$ and U_s' are in the same direction. Increased wind and wave activity can be seen several times during the period of observation. For example, wind activity peaked around hour 55 and the wave activity slightly later, with the resulting Langmuir number showing a prominent peak at around hour 60. Unfortunately, microstructure measurements are not available during this period (see Fig. 5). Several other peaks in Langmuir number can also be seen, for example at around hour 100.

The evolution of the model *T*, *S* structure in the water column for the base case (Case 4) with both wave breaking and shear production is shown in the upper two panels of Fig. 4, and the observed *T*, *S* structure in the bottom two panels. The agreement between the two is quite good, indicating that the *T*, *S* assimilation has been carried out successfully. Note also that the model successfully bridges the short dropout in CTD data (due to quality control)

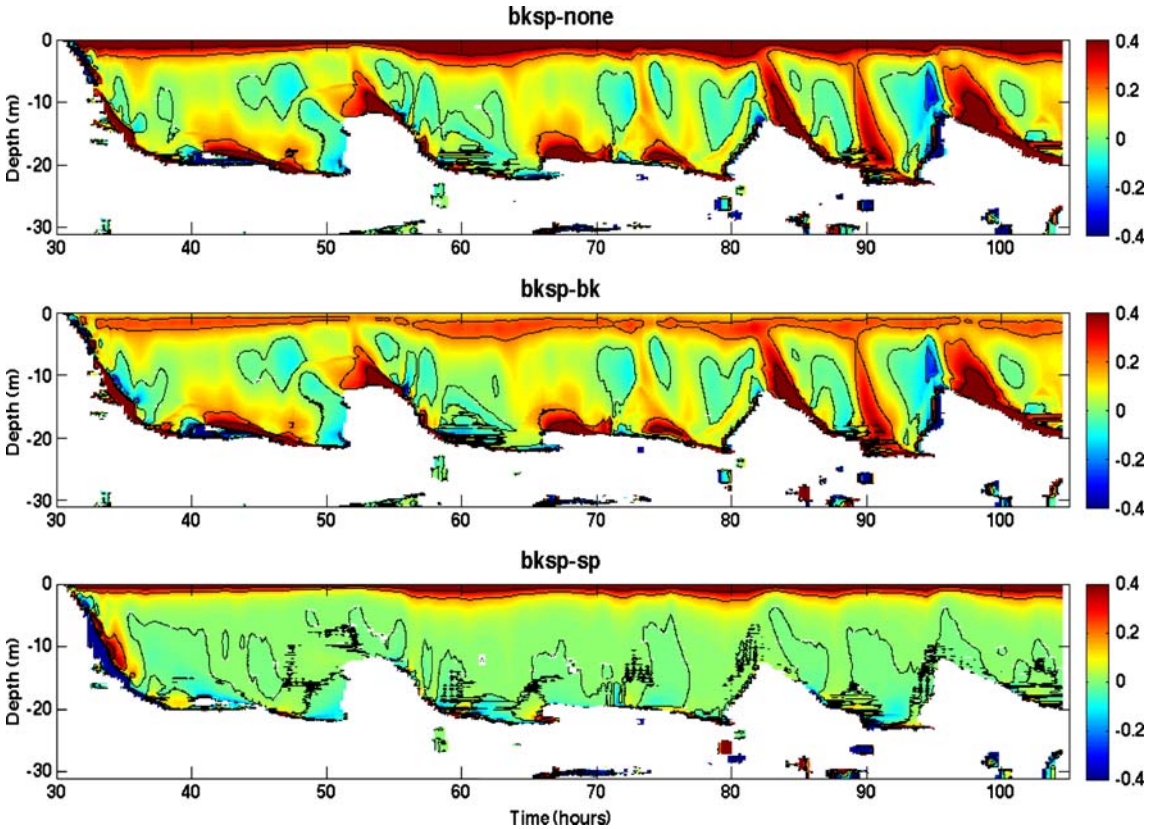

Fig. 7 The difference in the logarithm of the modeled TKE dissipation rates (in W kg^{-1}): (*top panel*) between Case 4 (with both wave breaking and Stokes production) and Case 1 (without either wave breaking or shear production), (*middle panel*) Case 4 and Case 2 (with wave breaking only), (*bottom panel*) Case 4 and Case 3 (with Stokes production only)

around hour 42. The *T*, *S* structure clearly shows a strong pycnocline at the base of the mixed layer at a depth of about 22 m. Since the pycnocline inhibits any deeper turbulence penetration into the water column, the upper bound on the mixed layer depth can also be expected to be around 22 m.

Figure 5 compares the temporal evolution of the observed TKE dissipation rate in the water column to the modeled rate for Case 4. Recall that the model includes both TKE injection at the surface by wave breaking and Stokes production of TKE in the interior of the water column. Note also that it is the logarithm of the dissipation rate that is plotted as a function of time. The agreement between the two is quite good, suggesting that the model has skill enough for use in estimating the Stokes production of TKE. The elevated dissipation rates near the air-sea interface are notable features in both observations and the model. The use of ascending microstructure profiler made it possible to measure the dissipation rate until the probes broke the surface. The top few meters would have been lost if measurements had been made using a conventional freely falling profiler. Dissipation rates are at least four orders of magnitude higher near the surface (of the order of 10^{-4} W kg^{-1}) than near the base of the mixed layer (of the order of 10^{-8} W kg^{-1}), and the model appears to reproduce the enhanced dissipation rate quite well. Unfortunately, microstructure data are missing between hours 53 and 60, precisely when the heightened wind and wave activity can be expected to produce higher TKE in the mixed layer. The same is true for the period between hours 73 and 79.5, but other periods of higher wind and wave activity (see Fig. 3) are covered by microstructure observations.

Figure 6 compares the modeled dissipation rates without wave breaking and Stokes production (Case 1) to the earlier-mentioned model results for Case 4. TKE injection at the surface is essential to reproduce the elevated dissipation rates near the surface. The strong mean shear near the surface, by itself, is not capable of elevating the dissipation rates to anywhere near the observed values. The near-surface values are of the order of 10^{-4} W kg^{-1} with additional TKE injection by waves. Wave-turbulence interaction cannot therefore be ignored in mixed layer models.

Figure 7 shows the difference in the logarithm of the dissipation rates between the base case (Case 4, wave breaking and Stokes production) and the other three cases. The top panel shows the difference between Cases 4 and 1 (neither wave breaking nor Stokes production), the middle panel, the difference between Cases 4 and 2 (wave breaking only), and the bottom panel, the difference between Cases 4 and 3 (Stokes production only). The top panel thus shows the influence of both wave breaking and Stokes production.

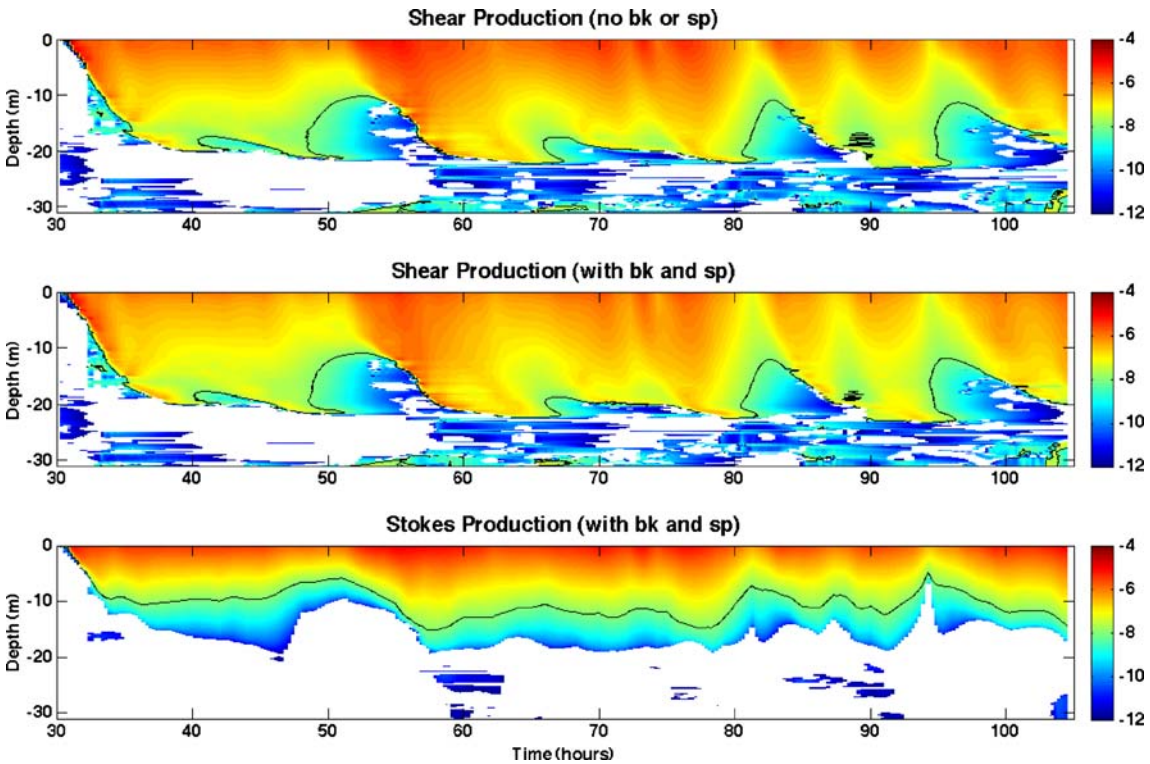

Fig. 8 Shear production of TKE (*top two panels*) and Stokes production of TKE (*bottom panel*) shown in logarithmic scale (in W kg^{-1}). The *top panel* is for the case without wave breaking or Stokes production (Case 1). *Middle panel* shows shear production when both are included (Case 4). The *bottom panel* shows Stokes production for Case 4

Enhanced dissipation rates occur not only near the surface and the base of the mixed layer, but generally throughout the active mixed layer. Large enhancements, for example around hours 83, 90, and 98, when turbulence penetrates into the water column after the preceding shallowing episode. The middle panel shows that Stokes production enhances dissipation rates generally throughout the active mixed layer, with large enhancements seen in the top panel around hours 83, 90, and 98 still intact. The surface enhancement is however, weaker, since wave-breaking effect is canceled out. The bottom panel shows that the dissipation rate enhancement is confined mainly to the near-surface layers (depths of about 2–3 m), since the effect of Stokes production is canceled out. The model results in Fig. 7 reinforce the commonly held notion (e.g., see Kantha and Clayson 2004) that while the influence of TKE injection by breaking surface waves is confined mainly to near-surface layers a few meters in depth, the Stokes production of TKE can affect the turbulence in the entire active mixed layer. It is also clear that both wave breaking and Stokes production must be included in the model to assure reasonable model fidelity.

Finally, Fig. 8 compares the shear production of TKE to the Stokes production of TKE. Shear production in the water column is shown, without wave breaking or Stokes production in the top panel, and with both in the middle panel. Comparison of these two panels indicates that including wave breaking and Stokes production produces only minor changes in shear production. This is interesting since additional TKE injection, whether in the near-surface layers by wave-breaking or in the interior of the active mixed layer by Stokes production, has the potential to modify both the turbulence and the mean shear in the water column, and therefore the shear production itself. The model simulations suggest that any such modifications are rather small. The bottom panel shows Stokes production in the water column for Case 4. Comparison of the middle and bottom panels indicates that the Stokes production of TKE in the water column is comparable in magnitude to the conventional shear production of TKE. The magnitudes of both can reach nearly 10^{-4} W kg^{-1}. This reinforces the idea that it is important to include Stokes production in a mixed layer model for realistic depiction of mixing in the OML. Note however that shear production penetrates deeper into the mixed layer (middle panel) than the Stokes production does (bottom panel). This is not surprising in view of the fact that the magnitude of the Stokes drift velocity decays exponentially with depth and so does the shear associated with it. Since both the turbulent shear stress and the shear of the Stokes drift are essential for Stokes production, Stokes production can be expected to be confined to the active mixed layer and moreover, to decrease rapidly with depth.

5 Concluding remarks

Recent rigorous theoretical work on wave-current-turbulence interactions in the ocean (Ardhuin et al. 2008), using the generalized Lagangian-mean approach of Andrews and McIntyre (1978), has confirmed that the surface gravity waves and the turbulence in the OML interact through the Stokes production term (Eq. 2), first included in OML models by Kantha and Clayson (2004). This term acts as a sink term for the waves and a source term for the turbulence. As such, it affects both the surface wave and oceanic mixed layer dynamics. As demonstrated in this study, the Stokes production of TKE can be similar in magnitude to that of the conventional shear production. It is therefore essential to include it in OML models for more accurate simulations of properties in the OML.

Unfortunately, it is difficult to measure Stokes production directly and it has to be inferred at present through a mixed layer model. Until recently, observational data needed to quantify Stokes production were not available. The Baltic Sea Research Institute Reynolds campaigns in the Baltic Sea provided the dataset needed to estimate Stokes production in the upper mixed layer.

The Reynolds 02 dataset is the only dataset we know of that makes a study such as this possible. Needless to say, more such campaigns would be useful in promoting a better understanding of Stokes production and its impact on mixing in the oceanic mixed layer. Better yet, direct measurement of turbulent shear stresses in the upper ocean should be made, which, along with measurement of the directional wave spectrum would enable direct measurement of Stokes production of TKE.

References

Andrews DG, McIntyre ME (1978) An exact theory of nonlinear waves on a Lagrangian-mean flow. J Fluid Mech 89:609–646

Ardhuin F, Rascle N, Belibassakis KA (2008) Explicit wave-averaged primitive equations using a generalized Lagrangian mean. Ocean Model 20:35–60

Carniel S, Sclavo M, Kantha LH, Clayson CA (2005) Langmuir cells and mixing in the upper ocean. Nuovo Cimento Soc Ital Fis C 28:33–54

Galperin B, Kantha LH, Hassid S, Rosati A (1988) A quasi-equilibrium turbulent energy model for geophysical flows. J Atmos Sci 45:55–62

Hasselmann K (1970) Wave-driven inertial oscillations. Geophys Fluid Dyn 1:463–502

Kantha L (2006) A note on the decay rate of swell. Ocean Model 11:167–173

Kantha LH, Clayson CA (1994) An improved mixed layer model for geophysical applications. J Geophys Res 99(C2):25, 235-25,266

Kantha LH, Clayson CA (2004) On the effect of surface gravity waves on mixing in the oceanic mixed layer. Ocean Model 6:101–124

Kantha L, Wittmann P, Sclavo M, Carniel S (2009) A preliminary estimate of the Stokes dissipation of wave energy in the global ocean. Geophys Res Lett 36:L02605. doi:10.1029/2008GL036193

Lass HU, Prandke H (2003) A study of the turbulent mixed layer in the Baltic Sea. In Chmielewski F-M, Foken T (eds) Beiträge zur Klima- und Meeresforschung. Berlin und Bayreuth, pp 159–168

Lass HU, Prandke H, Liljebladh B (2003) Dissipation in the Baltic proper during winter stratification. J Geophys Res 108(C6):3187. doi:10.1029/2002JC001401

McWilliams JC, Sullivan PP, Moeng C-H (1997) Langmuir turbulence in the ocean. J Fluid Mech 334:1–30

Mellor GL, Yamada T (1982) Development of a turbulence closure model for geophysical fluid problems. Rev Geophys 20:851–875